Structure, optical and visible-light photocatalytic performance of $Mo_{1-x}Co_xS_2$ ($0 \leq x \leq 0.1$) nanoparticles synthesized by facile hydrothermal method for methylene blue dye degradation

A. A. El-Fadl[a,b,*], M. A. M. Hussien[a, b], A. S. Soltan[a], A. Abu-Sehly[a,b]
[a]*Physics Department, Faculty of Science, Assiut University, 71516 Assiut, Egypt*
[b] *Lab. of Smart Materials for Energy Futures, Physics Department, Faculty of Science, Assiut University, 71516 Assiut, Egypt*

$Mo_{1-x}Co_xS_2$ ($0 \leq x \leq 0.1$) nanoparticles were successfully synthesized by using a hydrothermal route. The crystal structure of the prepared samples was investigated by X-ray diffraction (XRD), emphasizing that all the prepared samples had a hexagonal structure of MoS_2, and revealed an increment in the average particle size from 5 to 8 nm with increasing the cobalt ratio. The morphology was examined using scanning electron microscopy (SEM), and the recorded images of pure and cobalt-doped MoS_2 show flower-like architecture clusters. FT-IR spectroscopy was carried out to detect functional groups and stretching and bending vibrations of chemical bonds existing in all the prepared samples, confirming the presence of Mo-O and Co-O-Co characteristic peaks. The chemical composition of the synthesized samples was determined by energy dispersive X-ray (EDX) analysis. The results confirmed the presence of Mo, S, and Co, which are consistent with the proposed formation of $Mo_{1-x}Co_xS_2$ nanosystems. Optical properties were examined by UV–Visible spectrophotometry, reflecting allowed direct transitions with an energy band gap that decreases from 1.9 eV to 1.53 eV with increasing cobalt concentration. The photocatalytic degradation efficiency of methylene blue (MB) using pure and different ratios of cobalt-doped MoS_2 as catalysts was tested under visible light radiation, and it was noticed that the MB degradation increased with increasing cobalt concentration.

(Received September 20, 2023; Accepted January 8, 2024)

Keywords: MoS_2, Cobalt doped-MoS_2, X-ray diffraction, Morphology, Optical, SEM, FT-IR, EDX, Photocatalysis, Methylene blue degradation

1. Introduction

Environmental pollutants have increased in a terrible way in the last few decades as a result of industrial development, overpopulation, the use of chemical products such as pesticides and cosmetics, and the irresponsible behaviors of humans towards the nature. The disposal of dyes resulting from the factories of the textile sector in the water drains is one of the biggest causes of water pollution [1]. It is also expected that the number of harmful wastes that are released into the freshwater will reach 200 kilotons per year, most of which are toxic organic wastes, without any treatment or purification [2]. One of these harmful wastes is the methylene blue dye, which is used in numerous industries such as printing papers, advertisements, leather, and clothes coloring, and it is responsible for various sorts of diseases such as liver malfunctioning, skin irascibilities, and cancer [3].

Experimentally, purification of water from organic pollutants, salt, and other contaminants is expensive and consumes time [4]. Therefore, over the years, scientists have developed several techniques by which organic compounds and dyes can be removed from industrial wastewater, such as electrolysis, catalysis, photocatalysis, ion exchange, disinfection, microbial control, carbon filtering, membrane filtration, and reverse osmosis [3-5]. The photocatalysis technique plays a pivotal role among the aforementioned techniques in the degradation of pollutants because it is

* Corresponding author: abulfadla@yahoo.com
https://doi.org/10.15251/DJNB.2024.191.65

relatively low-cost, effective, and biologically safe [3, 6]. Semiconductors are among the active materials that are used in photocatalysis, but their effectiveness is limited and triggered by the ultraviolet region (5% of natural light) as a result of the relatively large optical band gap, as in the case of TiO_2 (E_g = 3.2 eV) [7]. This led to several attempts by the researchers to adjust the optical band gap of semiconductors to be active materials for photocatalysis in the region of visible light (45% of natural light) or to synthesize new active materials like transition metal dichalcogenides (TMDs) [7].

MoS_2 is one of the most important members of the TMD family. It has photochemical activity, mechanical stability, and unique magnetic, electronic, and optical properties that make it an active material for many applications, among them water purification [8, 9] and water splitting [10, 11]. Bulk MoS_2 shows slow and weak photocatalytic behavior due to its indirect band gap (E_g = 1.2 eV) and low active sites [12]. On the other side, stacked-layered MoS_2 has a direct optical band gap of 1.9 eV, which makes it very appropriate for photocatalysis in the visible light region [13]. According to the atomic coordination and stacking variations of MoS_2, it has three main phases: 1T, 2H, and 3R, where T, H, and R refer to tetragonal, hexagonal, and rhombohedral symmetry, respectively, while 1, 2, and 3 are the number of MoS_2 formulas in each unit cell [14]. The most prevalent structure that naturally exists is the semiconducting 2H-MoS_2, which is stable at room temperature [14]. Layers of MoS_2 are held together through weak van der Waal forces; these layers are created by covalent bonds between molybdenum and sulfur, S-Mo-S, as a Mo layer sandwiched between two S layers [15].

Morphological control is a very important parameter in reducing the limitation of MoS_2 usage in photocatalysis, despite its aforementioned unique features. This is because the photocatalytic activity depends on the abundance of edge sites and recombination time [16]. It is worth noting herein that morphological control is not the only strategy to achieve this reduction, but there are many other ways, including the insertion of amorphous-state MoS_2 with vacant Mo and S domains [17], making surface defects [18], and increasing the interlayer spacing [19].

Several techniques can be followed to synthesize MoS_2 nanoparticles, such as chemical vapor deposition [20], ultrasonic spray pyrolysis [21], sulfurization [22], liquid exfoliation [23], and decomposition of ammonium tetrathiomolybdate [24]. However, these techniques require complex equipment and high temperatures and are difficult to use, making it challenging to control the size and surface of MoS_2. Therefore, the bottom-up hydrothermal technique is convenient and effective for preparing and controlling the surface and size of nanomaterials without requiring high temperatures or complex procedures [25]. Hydrothermal technique also has many applications, such as hydrodesulfurization [21], lithium-ion battery [26], and hydrogen evolution reaction [27].

Latterly, doping semiconducting P-type MoS_2 with various transition metal ions has become an effective strategy to enhance its photocatalytic activity due to the greater number of active sites that can be created as a result of the doping process [20]. Farooq et al. [28] achieved 96% degradation efficiency of MB using 5% cadmium-doped MoS_2 with urea as a surfactant in 180 minutes. Li et al. [29] reported that the activation of peroxymonosulfate (PMS) by visible-light irradiation resulted in 92% tetracycline hydrochloride (TCH) degradation efficiency in 60 minutes for the as-prepared Fe-MoS_2 (0.1). Khan et al. [30] enhanced the photocatalytic activity of MoS_2 using nickel metal ions as a dopant; as the concentration of Ni doped in MoS_2 increased from 1% to 5%, the degradation of MB dye increased from 85% to 96% using a 500-watt Hg lamp as a source of UV radiation for 240 minutes. Their results showed that Ni doping enhanced the MB dye degradation process. In the same work, they also improved the degradation of Rhodamine B (RhB) dye under the same conditions from 77% to 91% with 1% to 5% Ni doping in MoS_2, compared to 62% for pure MoS_2.

MoS_2 has attracted much attention for both primary research and device fabrication, such as photodetectors [31]. Nano-MoS_2 is known for its high catalytic activity, chemical stability, low cost, and ease of synthesis. Its photocatalytic activity depends on its nanostructure and the number of exposed edge sites. Nevertheless, the drawbacks of MoS_2 as a photocatalyst are its water insolubility and small specific surface area. Hence, it's important to explore various techniques to increase the active sites in order to enhance its photocatalytic activity [32, 33]. In this study, the $Mo_{1-x}Co_xS_2$ ($0 \leq x \leq 0.1$) nanosystem has been synthesized via the facial hydrothermal technique to investigate its activity in photocatalytic application under visible light illumination. It was

expected that Co ions intercalation would not be difficult because of the comparable ionic radii of Mo^{+4} (65 pm) and Co^{+3} (54 pm) [34].

2. Experimental details

2.1. Materials

Superior purity chemicals such as ammonium molybdate tetrahydrate ($(NH_4)_6Mo_7O_{24}\cdot 4H_2O$), thiourea ($CH_4N_2S$), cobalt nitrate hexahydrate ($Co(NO_3)_2.6H_2O$), ethyl alcohol (CH_3CH_2OH), and methylene blue dye ($C_{16}H_{18}ClN_3S$) were provided by the ALPHA CHEMIKA company, and all the chemicals were used without any additional purification.

2.2. Synthesis of MoS_2 nanoparticles

Undoped MoS_2 nanoparticles were synthesized via a simple hydrothermal technique. In this experiment, 1.24 g of ($(NH_4)_6Mo_7O_{24}\cdot 4H_2O$) and 1.645 g of CH_4N_2S were dissolved in 30 ml of distilled water until a clear mixture was formed after stirring it for 30 min. The mixture was then put in a 40-ml Teflon-lined autoclave and heated at 210 °C for 24 h. After letting the sample cool naturally to room temperature, the black product was collected by a 4000 RPM centrifuge and washed many times with deionized water and ethanol. Finally, the product was dried in the oven at 60 °C for 12 h [35].

2.3. Synthesis of Co-doped MoS_2 nanoparticles

The synthesis of $Mo_{1-x}Co_xS_2$ ($0.02 \leq x \leq 0.1$) samples, with x varying in steps of 0.02, was performed using the hydrothermal route in the same procedure as for undoped MoS_2. The cobalt-doped material was produced in one step by adding stoichiometric weights of the reacting materials $(NH_4)_6Mo_7O_{24}\cdot 4H_2O$, Co $(No_3)_2.6H_2O$, and CH_4N_2S, with weight percentage in a 1-x: x: 2 ratio in the solution [36].

2.4. Photocatalytic experiment

Photocatalytic activity of the as-prepared and cobalt-doped MoS_2 nanoparticles was tested through MB dye degradation efficiency under the irradiation of visible light ($\lambda > 420$ nm). In this experiment, 10 mg of MoS_2 powder was added to 50 ml of a 10^{-5} molar aqueous solution of MB and stirred in the dark for 30 minutes to achieve adsorption-desorption equilibrium. Then, 3 ml of the suspended solution was gathered every 5-minutes interval to measure its absorbance spectrum up to 1000 nm via UV-Vis spectrophotometer [28]. The same steps are then repeated for each of the different cobalt-doped $Mo_{1-x}Co_xS_2$ samples, with varying Co ratios from x = 0.02 up to x = 0.10 in steps of 0.02, by adding 10 mg of each sample at a time.

3. Characterization and measurements

XRD patterns of the produced samples were recorded using Philips X-ray diffractometer of 1710 PW model, which based on CuK_α radiation (λ=1.54184 Å) and operates at 40 KV applied voltage. Angles between 5° and 80° were measured while maintaining an angle-scanning rate of 0.06° per minute. FT-IR transmittance spectra were performed using NICOLET FT-IR 6700 spectrometer in the range 400-4000 cm^{-1} for pellets samples mixed with KBr. In order to investigate the surface morphology of the prepared powder samples, SEM images were taken using (JSM)-T200 Jeol-Japan device. Elemental composition of the prepared samples was carried out using an energy dispersive X-ray spectroscopy (EDX) unit connected to a scanning electron microscope model ULTRADRY QUANTA FEG 250 (Field Emission Gun). Optical absorbance and catalytic curves were measured for the suspension nanoparticles using a Thermo Evolution 300 UV-Visible Spectrophotometer (200 to 1000 nm). Optical energy band gaps were calculated according to the Tauc plot from the UV- Visible data.

4. Results and discussion

4.1. X-ray diffraction

The microstructure of the hydrothermally prepared pure and cobalt-doped $Mo_{1-x}Co_xS_2$ ($0 \leq x \leq 0.1$) samples was examined by XRD analysis. The pattern appearing in figure 1.a shows six diffraction peaks positioned at 2θ = 13.78°, 28.72°, 33.22°, 39.28°, 48.87°, and 58.78° corresponding to (002), (004), (100), (103), (105), and (110) planes, respectively, which are in high agreement with standard data JCPDS file no. 37-1492, which reveals the formation of crystalline hexagonal MoS_2 (2H-MoS_2 polytype) without any impurities [37, 38]. All the doped samples with different cobalt concentrations (from x = 0.02 to x = 0.1) reflect the same peaks, which is clear evidence of stabilization of the hexagonal crystal structure without any formation of molybdenum oxide peaks such as MoO_3 or MoO_2 [39]. The inequality of the broadening of the reflected peaks, ranging from 0.3° to 3.3° for different hkl reflections, can be attributed to the presence of small grains with respect to others [34]. The average particle size can be calculated with the following Debye-Scherrer formula [40]:

$$D_{XRD} = \frac{k\lambda}{\beta \cos(\theta)} \quad (1)$$

Here β is the full width at half maximum, θ is Bragg's angle**,** k is the shape factor and here is considered to be 0.94, and λ is the wavelength (λ=0.154 nm).

The average particle size (D_{XRD}) for the $Mo_{1-x}Co_xS_2$ nanosystem is estimated, and it exhibits a systematic increase with increasing cobalt-doping concentration, as shown in figure 1.b. The lattice strain ε, dislocation density δ, and theoretical density ρ can be calculated according to equations (2), (3), and (4), respectively [41, 42].

$$\varepsilon = \frac{\beta}{4 \tan(\theta)} \quad (2)$$

$$\delta = \frac{1}{D^2} \quad (3)$$

$$\rho = \frac{ZM}{N_a V} \quad (4)$$

where Z is the number of formulas per unit cell (Z = 2 for MoS_2), M is the molecular weight, and N_a is Avogadro's number.

Also, the lattice volume V of the hexagonal structure can be calculated via equation (5) [43]. It was found that, the volume of the unit cell decreases with increasing the ratio of Co concentration, and this is due to decreasing the lattice parameters a and c of the hexagon, which can be explained in terms of the ionic radii difference for both Mo^{+4} (65 pm) and Co^{+3} (54 pm) [34]. The obtained parameters are indexed using the CellRef program [44], and the calculated data are listed in Table 1.

$$V = \frac{\sqrt{3}}{2} a^2 c \quad (5)$$

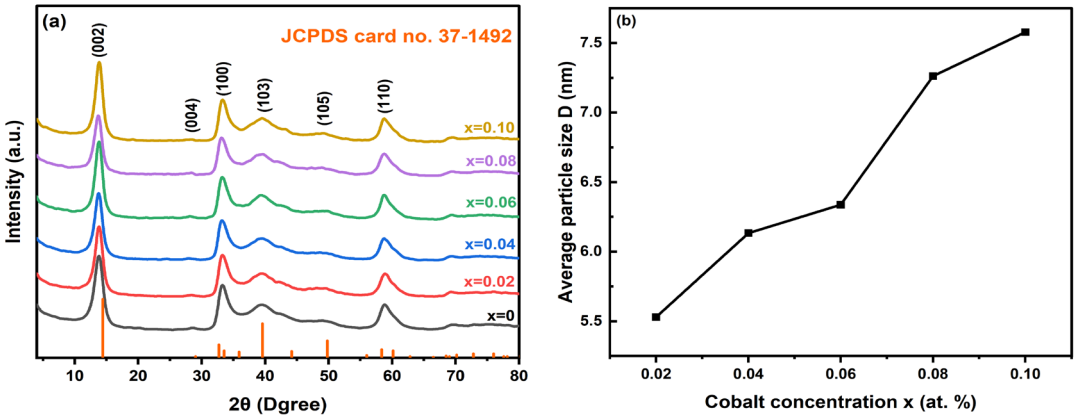

Fig. 1. (a) XRD diffraction patterns of $Mo_{1-x}Co_xS_2$ ($0 \leq x \leq 0.1$) nanoparticles; (b) change of the average particle size (D_{XRD}) with Co concentration.

Table 1. XRD-estimated structural parameters of Mo_{1-x} Co_x S_2 nanoparticles.

x	a (Å)	c (Å)	V (Å^3)	ρ (gm/cm^3)	D_{XRD} (nm)	$\varepsilon \times 10^{-2}$	$\delta \times 10^{-3}$ (nm)^2
0	3.149	12.604	108.27	4.909	8.083	2.468	4.259
0.02	3.149	12.539	107.67	4.914	5.529	2.689	4.909
0.04	3.148	12.448	106.82	4.931	6.134	2.664	5.584
0.06	3.146	12.352	105.87	4.952	6.336	2.529	4.580
0.08	3.140	12.403	105.92	4.926	7.262	2.440	4.465
0.10	3.148	12.328	105.82	4.908	7.578	2.672	6.016

4.2. Fourier Transform Infra-Red Spectroscopy

FT-IR spectroscopy was carried out to detect the stretching and bending vibrations of the chemical bonds existing in the prepared samples of the $Mo_{1-x}Co_xS_2$ system. As appears in figure 2, for the as-prepared MoS_2 (x = 0), there are transmittance peaks centered at 3458 cm^{-1}, 1629 cm^{-1}, 1405 cm^{-1}, 1090 cm^{-1}, 910 cm^{-1}, and 590 cm^{-1}. The band positioned at 3458 cm^{-1} is attributed to symmetrical (O-H) stretching vibration bonds, and the band position at 1629 cm^{-1} is credited to stretching vibrations (-OH) of the hydroxyl group [45]. While the peak located at 1405 cm^{-1} is due to characteristic (Mo-O) vibration [45]. The bands located at 1090 cm^{-1}, 910 cm^{-1}, and 590 cm^{-1} are assigned to S-O asymmetric stretching, S-S bond, and Mo-S vibration, respectively [45, 46]. In addition to the bands that appear in the pristine MoS_2, there are two peaks that appear in the cobalt-doped MoS_2 samples. The first one is positioned at 1205 cm^{-1} due to the presence of a C-S bond [46], and the other located at 760 cm^{-1} due to Co-O-Co functionalities [47, 48].

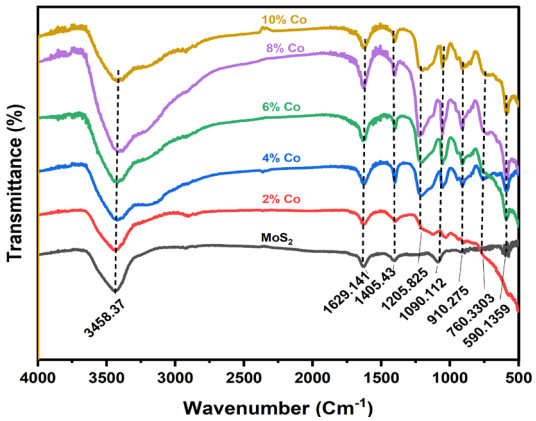

Fig. 2. FT-IR spectra of $Mo_{1-x}Co_xS_2$ nanosystem.

4.3. Scanning electron microscopy (SEM)

The morphological information of undoped and cobalt-doped MoS_2 samples was employed by scanning electron microscopy (SEM). The recorded image of pure MoS_2 presented in figure 3.a shows regular, flower-like architecture clusters. Higher magnification SEM images in figures 3.b and 3.c emphasize the 2D structure of these flower-like MoS_2, and each single nanoflower consists of tens to hundreds of slightly curved petals [36, 49]. When compared to pure MoS_2, the morphology and structure of cobalt-doped $Mo_{1-x}Co_xS_2$ samples that are shown in figures 3.(d-f) for 4%, 8%, and 10% cobalt ratios, one can notice several voids and less agglomeration appear in the images of these samples, which supply more beneficial active sites for catalytic reactions [50-52].

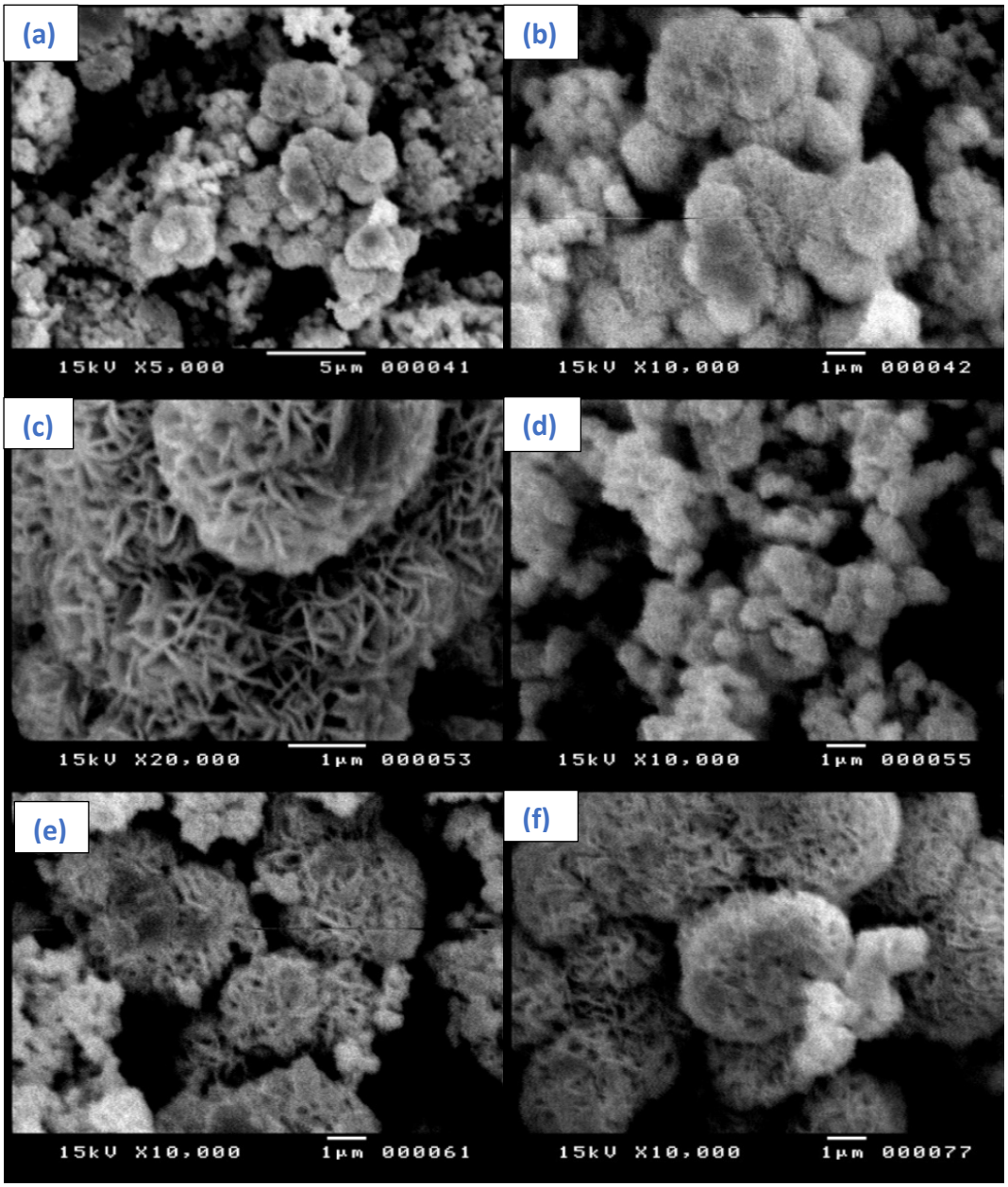

Fig. 3. (a-c) SEM images of undoped MoS_2; (d) 4% Co-doped MoS_2; (e) 8% Co-doped MoS_2; and (f) 10% Co-doped MoS_2.

4.4. Energy Dispersive X-Ray Spectroscopy (EDX)

Energy dispersive X-ray measurement was carried out to detect the chemical composition of the prepared $Mo_{1-x}Co_xS_2$ nanoparticles. Figures 4.(a-f) show only the peaks of molybdenum (Mo) and sulfur (S) for pure MoS_2 and the peaks of molybdenum (Mo), sulfur (S), and cobalt (Co) for cobalt-doped MoS_2 samples. These peaks reveal that no foreign impurity is detected. Molybdenum has its peak at 2.47 KeV, corresponding to L_α radiations, and sulfur has its peak at 2.48 KeV, corresponding to K_α radiations, while cobalt has its peaks at 6.91 KeV and 7.64 KeV corresponding to K_α and K_β radiations, respectively [28, 53]. The energy levels of sulfur and molybdenum are so close that their peaks are not distinct [28]. The detected Co, Mo, and S confirm the proposed formation of $Mo_{1-x}Co_xS_2$ nanosystems.

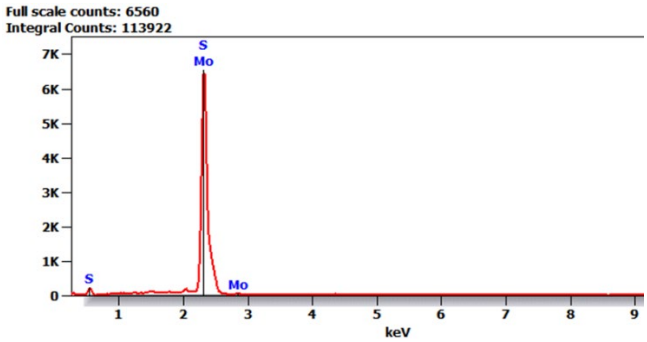

(a)

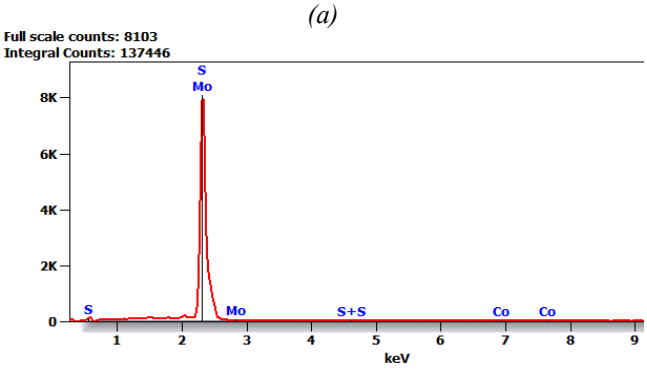

(b)

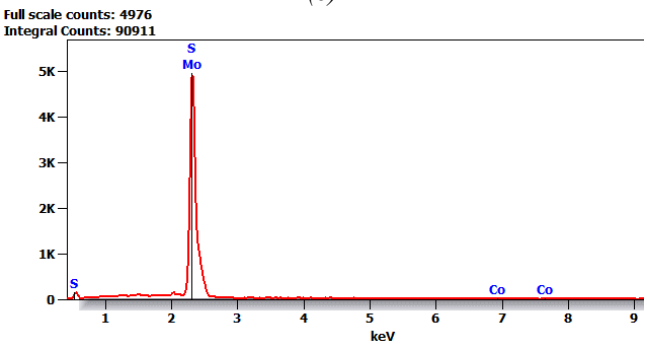

(c)

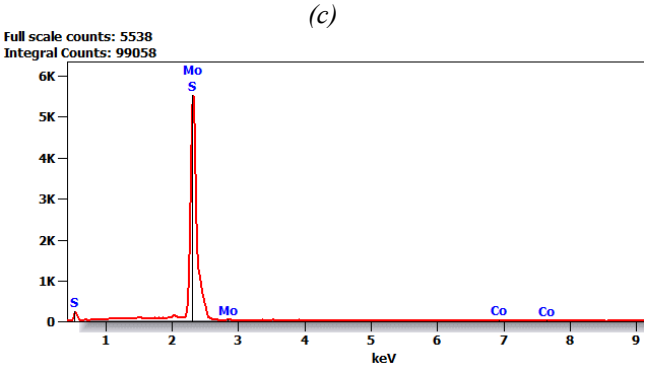

(d)

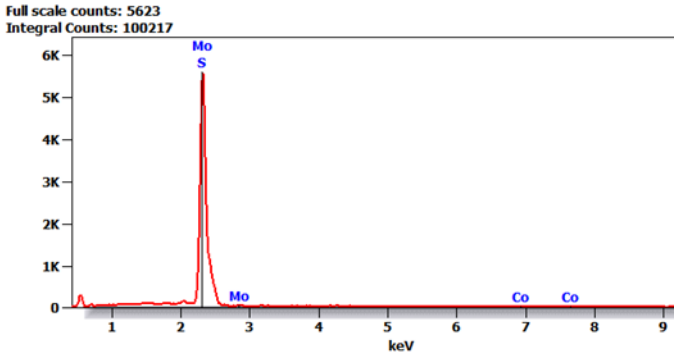

(e)

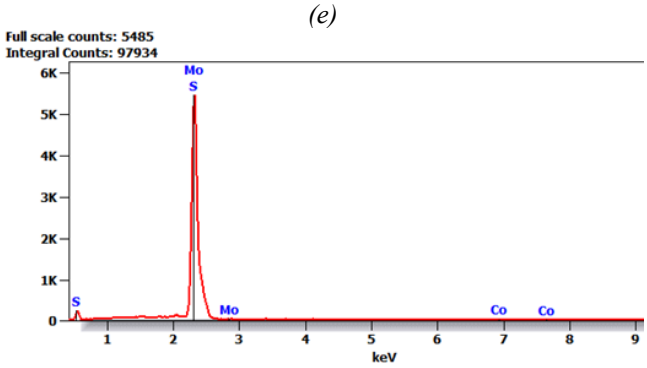

(f)

Fig. 4. EDX spectra of $Mo_{1-x}Co_xS_2$ nanosystem: (a) x = 0; (b) x = 0.02; (c) x = 0.04; (d) x = 0.06; (e) x = 0.08; and (f) x = 0.1.

4.5. Ultraviolet Visible Spectroscopy

The optical characteristics of pure MoS_2 and cobalt-doped MoS_2 nanoparticles dispersed in distilled water have been examined via UV-Vis absorption spectroscopy. Figure 5.a clarifies the absorbance spectra of undoped MoS_2. As observed, there are three bands, one in the range of 450-480 nm, and the other two absorption bands appear around 630 nm and 680 nm because the direct band gap transitions at the K point [54 ,55]. This is a good indication that MoS_2 nanoflowers have a small optical band gap (~1.8 eV) owing to the quantum confinement effect [56]. The absorption spectra of the different cobalt-doped concentrations of $Mo_{1-x}Co_xS_2$ ($0.02 \leq x \leq 0.1$) are shown in figure 5.b. Equation (6) can be used for the calculation of the absorption coefficient α [57]:

$$\alpha = \frac{2.303\rho\times10^3}{lcM}A \tag{6}$$

where A is the absorbance, ρ is the theoretical density of each sample, L is the optical path length here considered to be 1 cm, M is the mass of one mole, and c is the molar concentration.

The optical band gap of these samples can be calculated by applying Tauc equation [58],

$$(\alpha h\nu)^n = B\,(h\nu - E_g) \tag{7}$$

where α is the absorption coefficient in cm^{-1}, hν is the energy of the incident photons in eV, B is a constant independent of the photon energy, and n is a constant that may has one of four values 2, 1/2 and 3, 1/3 for direct, indirect allowed transition, and direct and indirect forbidden transition, respectively and E_g is the optical band gap. The exponential-like behavior for the obtained data appears at n = 2 (direct allowed transition) when plotted hν on the X-axis versus $(\alpha h\nu)^2$ on the Y-axis, while the value of the band gap could be detected by tacking the intercept of the fitting straight line as in figures 6.(a-f).

The calculated value of the optical band gap for pristine MoS_2 is E_g = 1.9 eV, which is similar to the result concluded in a previous work [59]. However, when we incorporated cobalt ions into the material's lattice by using the $Mo_{1-x}Co_xS_2$ nanoparticles, we observed a decrease in

the optical band gap by increasing the cobalt ratio. As a result, the optical band gap reached 1.53 eV for the 10% Co doping concentration, as shown in figure 7. This implies that adding Co as a dopant created high oxygen vacancies in the material, resulting in the formation of new energy states near the valence band top and conduction band bottom, which is consistent with the theoretical result obtained from DFT calculations [60].

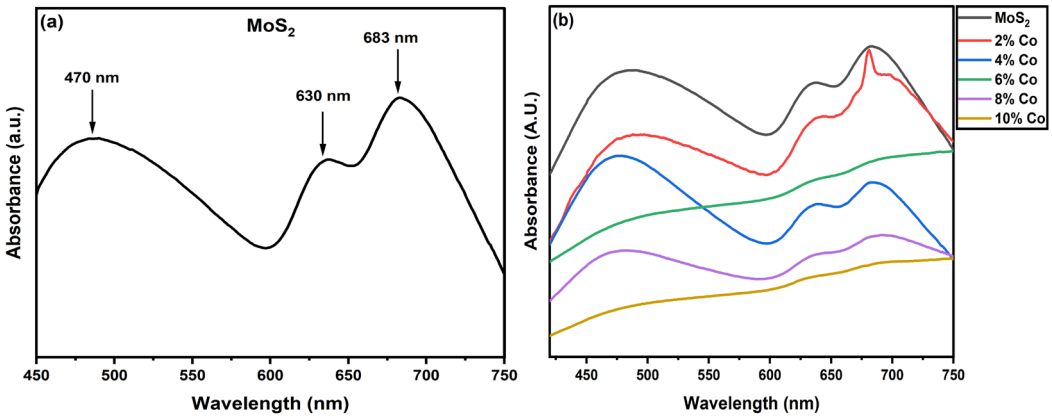

Fig. 5. UV-Vis absorption spectra of (a) pure MoS_2 and (b) cobalt-doped $Mo_{1-x}Co_xS_2$ system.

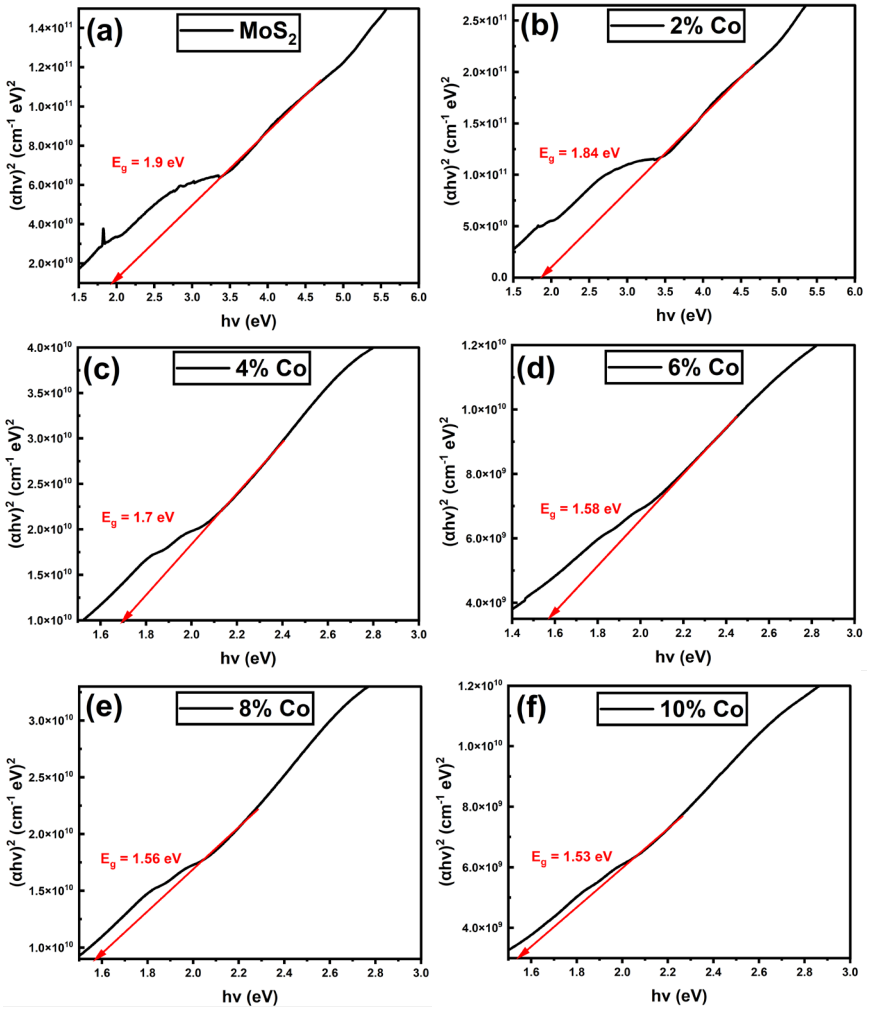

Fig. 6. Optical band gaps of $Mo_{1-x}Co_xS_2$ system with different Co doping concentrations, calculated using Tauc's plot. (a) x = 0; (b) x = 0.02; (c) x = 0.04; (d) x = 0.06; (e) x = 0.08; and (f) x = 0.1.

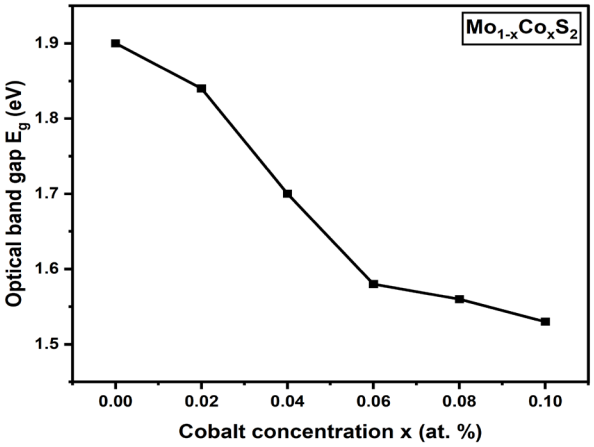

Fig. 7. Variation of the optical band gap with cobalt concentration through $Mo_{1-x}Co_xS_2$ nanosystem.

4.6. Photocatalytic studies

The photocatalytic dye degradation is explained in terms of the absorption of light by dye molecules in the investigated specimen. Figures 8. (a-g) show the sequential time-dependent UV-Vis spectra of photocatalytic degradation of MB under visible light irradiation. The degradation process was followed up by a gradual decrease in the main absorption peak of MB around 663 nm [61]. The degradation of MB without any catalyst was carried out as shown in figure 8.a, and no self-degradation was noticed over time. This ensures that the dye degradation process is solely dependent on the photocatalyst. The photocatalytic degradation efficiency (E%) for $Mo_{1-x}Co_xS_2$ ($0 \leq x \leq 0.1$) nanosystem samples was calculated by using the following equation [62]:

$$E\% = \frac{A_0 - A_t}{A_0} \times 100 \quad (8)$$

where A_0 and A are the absorption values determined by the UV-Visible spectrophotometer at 0 and t minutes, respectively.

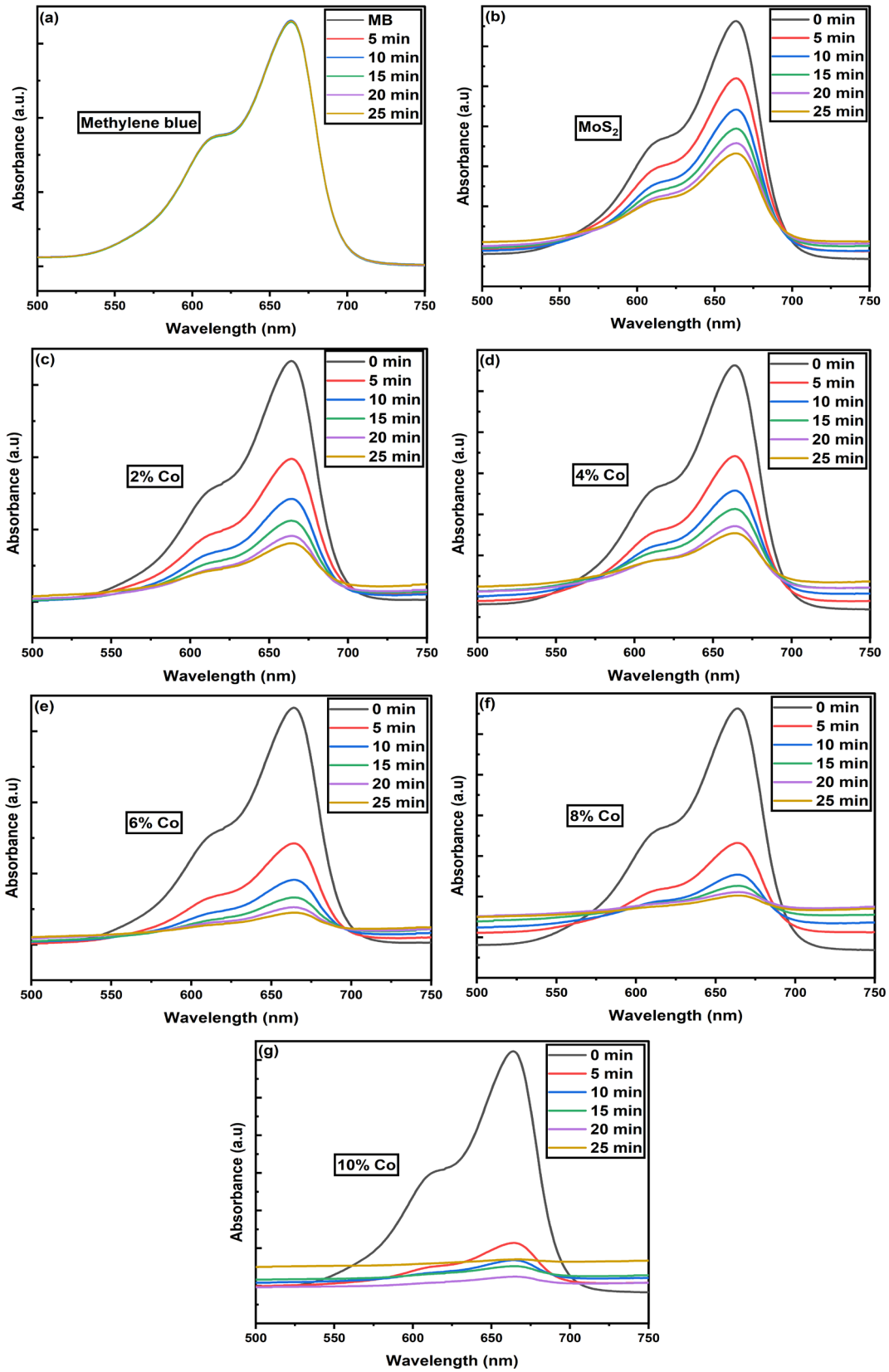

Fig. 8. Sequential time-dependent UV-vis spectra of photocatalytic degradation of MB under visible light irradiation in the presence of: (a) only MB dye; (b) pure MoS_2; (c) 2% Co doped MoS_2; (d) 4% Co-doped MoS_2; (e) 6% Co-doped MoS_2; (f) 8% Co-doped MoS_2; and (g) 10% Co-doped MoS_2.

Undoped MoS_2 has the lowest degrading activity (50%), indicating that pure MoS_2 has weak absorbance in the visible portion of the electromagnetic spectrum, which is in great agreement with the previous work indicated by Ye et al. [63]. The photocatalytic degradation was enhanced to 58.2%, 61.7%, 66.5%, 69.4%, and 82.8% by increasing the concentration of cobalt to 2%, 4%, 6%, 8%, and 10% Co, respectively, which means that the optimum photocatalyst concentration is 10% Co ($Mo_{0.90}Co_{0.1}S_2$). The enhancement of the photocatalytic properties of cobalt-doped MoS_2 over the pure one may be because doping increases the number of active MoS_2 sites and improves the separation of electron-hole pairs [64]. Figure 9.a reflects the change in the ratio of C_t/C_0 during the period of light irradiation. Furthermore, the Langmiur-Henshelwood (L-H) model, which is treated as a pseudo first-order kinetic reaction depicted in equation (9), is utilized to derive the recombination rate constant (γ) for MB dye [65].

$$\ln\left(\frac{C_t}{C_0}\right) = \gamma t \tag{9}$$

where C_0 is the dyes' initial concentration before illumination, C_t is the residual concentration at time t, and γ is the rate constant.

In order to study the kinetic reaction of MB degradation, the rate constant γ for all the synthesized samples is calculated by taking the slope of the lines in figure 9.b. The recombination rate constant γ and degradation efficiency E% of MB dye using $Mo_{1-x}Co_xS_2$ ($0 \leq x \leq 0.1$) nanoparticles are shown in figures 9.c and 9.d, respectively. Figure 10 displays the proposed photodegradation mechanism; moreover, the following few points summarize how MoS_2 degrades a dye [65]:

i. Light is absorbed by MoS_2, resulting in photogenerated electron hole pairs.

ii. These generated electrons in the conduction band interact with oxygen molecules present in water and form superoxide radicals $O_2^{\cdot -}$.

iii. Meanwhile, holes interact with water molecules, causing the formation of hydroxyl radicals.

iv. Finally, these radicals undergo a chemical reaction with the organic molecules that are in the dye, degrading them into H_2O and CO_2.

$$MoS_2 + h\nu \rightarrow MoS_2\,(e^- + h^+) \tag{10}$$

$$MoS_2(e^-) + O_2 \rightarrow O_2^{\cdot -} \tag{11}$$

$$MoS_2(h^+) + H_2O \rightarrow OH^{\cdot} + H^+ \tag{12}$$

$$O_2^{\cdot -} + H_2O \rightarrow H_2O_2 + OH \tag{13}$$

$$H_2O_2 \rightarrow 2\,OH^{\cdot} \tag{14}$$

$$OH^{\cdot} + Dye \rightarrow CO_2 + H_2O \tag{15}$$

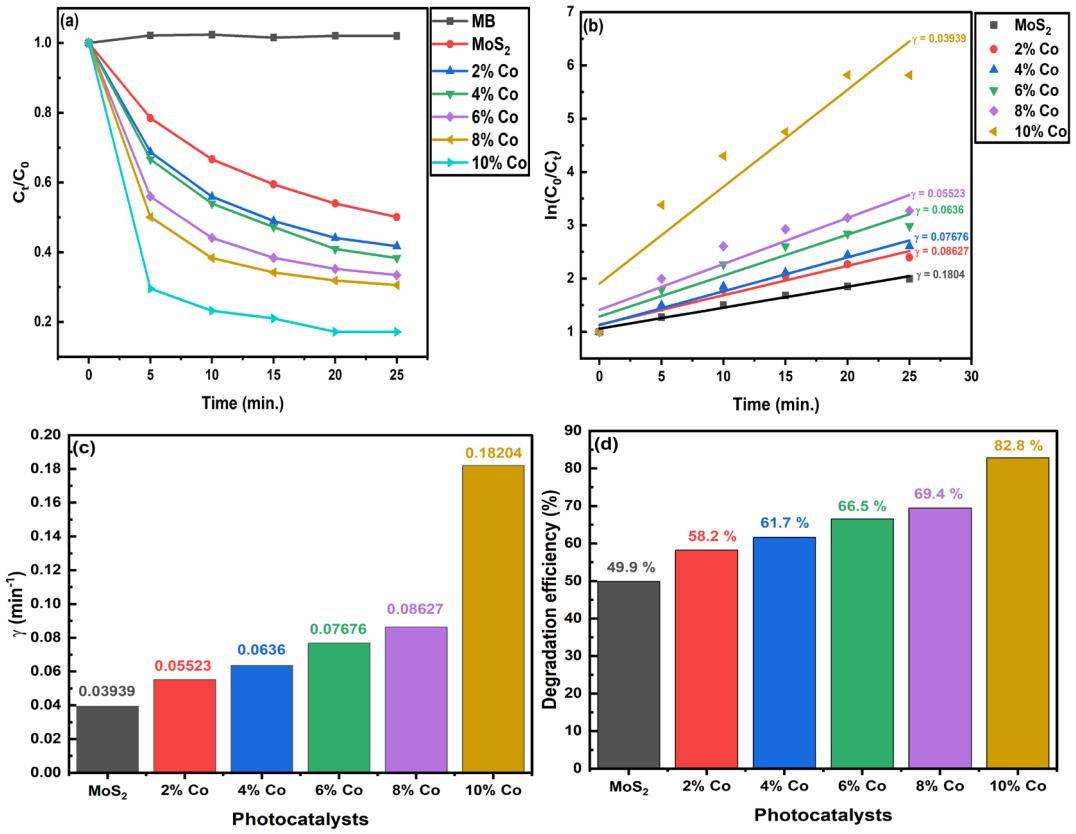

Fig. 9. (a) change in the ratio of C_t/C_0 versus the time of light irradiation; (b) ln (C_0/C_t) versus period for kinetic reaction; (c) recombination rate constant γ of $Mo_{1-x}Co_xS_2$ ($0 \leq x \leq 0.1$) for MB dye; and (d) MB photocatalytic degradation efficiency (E%) for all the $Mo_{1-x}Co_xS_2$ samples.

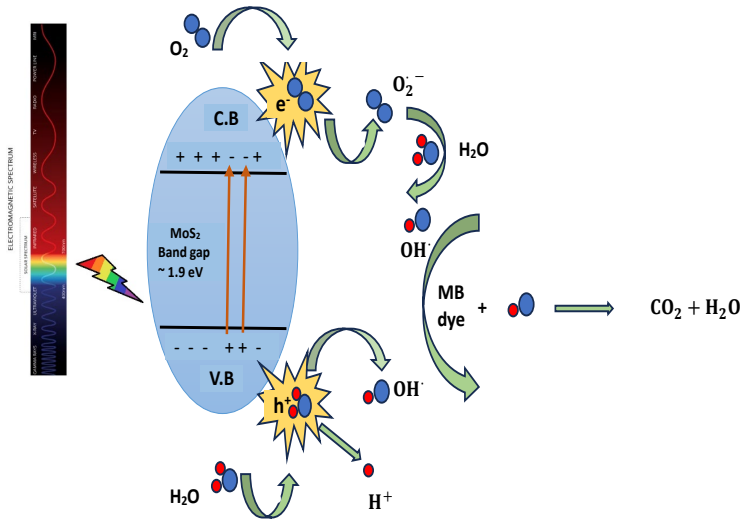

Fig. 10. Schematic description for the MB dye degradation mechanism in MoS_2 photocatalyst.

5. Conclusion

Hydrothermal process was successfully used to synthesize $Mo_{1-x}Co_xS_2$ ($0 \leq x \leq 0.1$) nanoparticles. XRD and FT-IR obviously demonstrate the formation of a single-phase

semiconducting undoped and cobalt-doped MoS_2. Lattice parameters decreased with increasing cobalt ion ratio because of its smaller ionic radius as compared to the radius of Mo ion. The average grain size was found to increase with the increase in cobalt percentage and ranged from 5 to 8 nm. SEM images establish the formation of 2D nanoflowers and show an increment in the gaps through the material with cobalt ratios, which supply more beneficial active sites for catalytic reactions. Detection of cobalt, molybdenum, and sulfur using energy dispersive X-ray spectroscopy (EDX) confirms the proposed formation of $Mo_{1-x}Co_xS_2$ nanosystems. UV-visible studies demonstrate that the optical band gaps decreased with increasing Co content, which is ascribed to the creation of sub-levels among the energy band gaps. This, in turn, affects the photocatalytic activity of $Mo_{1-x}Co_xS_2$ nanoparticles or the degradation of MB dye as the degradation becomes more efficient by increasing the Co-ion substitutions.

References

[1] Raman, C. Devi, S. J. J. E. M. Kanmani, Journal of Environmental Management, 177, 341 (2016); https://doi.org/10.1016/j.jenvman.2016.04.034

[2] B. Valley, B. Jing, M. Ferreira, Y. Zhu, ACS applied materials & interfaces, 11(7), 7472, (2019); https://doi.org/10.1021/acsami.8b21674

[3] M. Junaid, M. Imran, M. Ikram, M. Naz, M. Aqeel, H. Afzal, H. Majeed, S. Ali, Applied Nanoscience, 9, 1593, (2019); https://doi.org/10.1007/s13204-018-0933-3

[4] S. Dervin, D. D. Dionysiou, S. C. Pillai, Nanoscale, 8(33), 15115, (2016); https://doi.org/10.1039/C6NR04508A

[5] K. R. Kunduru, M. Nazarkovsky, S. Farah, R. P. Pawar, A. Basu, A. J. Domb, Water purification, chapter 2, 33-74, (2017); https://doi.org/10.1016/B978-0-12-804300-4.00002-2

[6] X. Zhang, H. Suo, R. Zhang, S. Niu, X. q. Zhao, J. Zheng, C. Guo, Materials Research Bulletin, 100, 249 (2018); https://doi.org/10.1016/j.materresbull.2017.12.036

[7] N. Rahimi, R. A. Pax, E. M. Gray, Progress in Solid State Chemistry, 44(3), 86, (2016); https://doi.org/10.1016/j.progsolidstchem.2016.07.002

[8] M. Heiranian1, A. B. Farimani, N. R. Aluru, Nature communication, 6(1), 8616, (2015); https://doi.org/10.1038/ncomms9616

[9] J. Kou, J. Yao, L. Wu, X. Zhou, H. Lu, F. Wu, J. Fan, Physical Chemistry Chemical Physics, (18),32, 22210, (2016); https://doi.org/10.1039/C6CP01967F

[10] P. Cheng, C. Yuan, Q. Zhou, X. Hu, J. Li, X. Lin, X. Wang, M. Jin, L. Shui, Xingsen Gao, R. Nötzel, G. Zhou, Z. Zhang, J. Liu, The Journal of Physical Chemistry C, 123(10), 5833, (2019); https://doi.org/10.1021/acs.jpcc.8b10954

[11] P. Gnanasekar, D. Periyanagounder, J. Kulandaivel, Nanoscale, 11(5), 2439, (2019); https://doi.org/10.1039/C8NR10092F

[12] Y. Okuno, O. Lancry, A. Tempez, C. Cairone, M. Bosi, F. Fabbri, M. Chaigneau, Nanoscale, 10(29), 14055, (2018); https://doi.org/10.1039/C8NR02421A

[13] G. Deokar, N. S. Rajput, P. Vancsó, F. Ravaux, M. Jouiad, D. Vignaud, F. Cecchetd, J.F. Colomera, Nanoscale, 9(1), 277, (2017); https://doi.org/10.1039/C6NR07965B

[14] O. Samy, A. ElMoutaouakil, Energies, 14(15), 4586, (2021); https://doi.org/10.3390/en14154586

[15] Z. Dai, W. Jin, M. Grady, J. T. Sadowski, J. I. Dadap, R. M. Osgood, K. Pohl, Surface Science, 660, 16, (2017); https://doi.org/10.1016/j.susc.2017.02.005

[16] H. K. Sadhanala, S. Senapati, K. V. Harika, K. K. Nanda, A. Gedanken, New Journal of Chemistry, 42(17), 14318, (2018); https://doi.org/10.1039/C8NJ01731J

[17] C. G. Morales-Guio, X. Hu, Accounts of chemical research, 47(8), 2671, (2014); https://doi.org/10.1021/ar5002022

[18] U. Xie, H. Zhang, S. Li, R. Wang, X. Sun, M. Zhou, J. Zhou, X. W. Lou, Y. Xie, Advanced materials, 25(40), 5807, (2013); https://doi.org/10.1002/adma.201302685

[19] M. R. Gao, M. K.Y. Chan, Y. Sun, Nature communications, 6(1), 7493, (2015).
[20] X. Wang, H. Feng, Y. Wu, L. Jiao, Journal of the American Chemical Society, 135(14), 5304, (2013); https://doi.org/10.1021/ja4013485
[21] S. E. Skrabalak, K. S. Suslick, Journal of the American Chemical Society, 127(28), 9990, (2005); https://doi.org/10.1021/ja051654g
[22] H. A. Therese, N. Zink, U. Kolb, W. Tremel, Solid state sciences, 8(10), 1133, (2006); https://doi.org/10.1016/j.solidstatesciences.2006.05.011
[23] D. Gopalakrishnan, D. Damien, M. M. Shaijumon, ACS nano, 8(5), 5297, (2014); https://doi.org/10.1021/nn501479e
[24] N. Li, Y. Chai, Y. Li, Z. Tang, B. Dong, Y. Liu, C. Liu, Materials Letters, 66(1), 236, (2012); https://doi.org/10.1016/j.matlet.2011.08.092
[25] L. Ma, W. Chen, H. Li, Y. Zheng, Z. Xu, Materials Letters, 62(6-7), 797, (2008); https://doi.org/10.1016/j.matlet.2007.06.062
[26] Y. Gong, S. Yang, Z. Liu, L. Ma, R. Vajtai, P. M. Ajayan, Advanced materials, 25(29), 3979, (2013); https://doi.org/10.1002/adma.201301051
[27] D. Merki, X. Hu, Environmental Science, 4(10), 3878, (2011); https://doi.org/10.1039/c1ee01970h
[28] M. Farooq, T. Iqbal, Journal of Inorganic and Organometallic Polymers and Materials, 32(11), 4422, (2022); https://doi.org/10.1007/s10904-022-02428-4
[29] Z. Li, M. Sun, J. Yang, S. Dong, Chemical Engineering Journal, 446, 137380, (2022); https://doi.org/10.1016/j.cej.2022.137380
[30] M. Khan, M. S. Hasan, K. A. Bhatti, H. Rizvi, A. Wahab, S. Rehman, M. J. Afzal, A. Nazneen, M. F. khan, A. Nazir, M. Iqbal, Effect of Ni doping on the structural, Materials Research Express, 7(1), 015061, (2020); https://doi.org/10.1088/2053-1591/ab66f7
[31] A. Taffelli, S. Dirè, A. Quaranta, L. Pancheri, Sensors, 21(8), 2758, (2021); https://doi.org/10.3390/s21082758
[32] R. Abinaya, J. Archana, S. Harish, M. Navaneethan, S. Ponnusamy, C. Muthamizhchelvan, M. Shimomurad, Y. Hayakawa, RSC advances, 8(47), 26664, (2018); https://doi.org/10.1039/C8RA02560F
[33] Y. Jiang, D. Wang, J. Li, M. Li, Z. Pan, H. Ma, G. Lv, W. Qu, L. Wang, Z. Tian, Catalysis Science & Technology, 7(14), 2998, (2017); https://doi.org/10.1039/C7CY01026E
[34] R. Sanikop, S. Gautam, K. H. Chae, C. Sudakar, Journal of Magnetism and Magnetic Materials, 537, 168226, (2021); https://doi.org/10.1016/j.jmmm.2021.168226
[35] K. Krishnamoorthy, G. K. Veerasubramani, S. Radhakrishnan, S. J. Kim, Materials Research Bulletin, 50, 499, (2014); https://doi.org/10.1016/j.materresbull.2013.11.019
[36] P. Chena, Y. Gou, J. Ni, Y. Liang, B. Yang, F. Jia, S. Song, Chemical Engineering Journal, 401, 125978, (2020); https://doi.org/10.1016/j.cej.2020.125978
[37] L. Chacko, P. K. Rastogi, P. M. Aneesh, Journal of The Electrochemical Society, 166(8), H263, (2019); https://doi.org/10.1149/2.0071908jes
[38] P. Chen, S. Zeng, Y. Zhao, S. Kang, T. Zhang, S. Song, Journal of Materials Science & Technology, 41, 88, (2020); https://doi.org/10.1016/j.jmst.2019.09.021
[39] V. Forsberg, R. Zhang, J. Bäckström, C. Dahlström, B. Andres, M. Norgren, M. Andersson, M. Hummelgård, H. Olin, PloS one, 11(4), e0154522, (2016); https://doi.org/10.1371/journal.pone.0154522
[40] A. O. Bokuniaeva, A. S. Vorokh, In journal of physics: Conference series, 1410(1), 012057, (2019); https://doi.org/10.1088/1742-6596/1410/1/012057
[41]. D. Nath, F. Singh, R. Das, Materials Chemistry and Physics, 239, 122021, (2020); https://doi.org/10.1016/j.matchemphys.2019.122021
[42]. A. Abu El-Fadl, M.I. Abd-Elrahman, Noha Younis, N. Afify, A.A. Abu-Sehly, M.M. Hafiz, Journal of Alloys and Compounds, 795, 114, (2019); https://doi.org/10.1016/j.jallcom.2019.05.008
[43]. K. Ravichandran, K. Karthika, B. Sakthivel, N. J. Begum, S. Snega, K. Swaminathan, V.

Senthamilselvi, Journal of magnetism and magnetic materials, 358, 50, (2014); https://doi.org/10.1016/j.jmmm.2014.01.008

[44] http://mill2.chem.ucl.ac.uk/tutorial/lmgp/celref.htm

[45] A. Raza, M. Ikram, M. Aqeel, M. Imran, A. Ul-Hamid, K. N. Riaz, S. Ali, Applied Nanoscience, 10, 1535, (2020); https://doi.org/10.1007/s13204-019-01239-3

[46] R. Rahman, D. Samanta, A. Pathak, T. K. Nath, RSC advances, 11(3), 1303, (2021); https://doi.org/10.1039/D0RA08229E

[47] S. Haq, F. Abbasi, M. Ben Ali, A. Hedfi, A. Mezni, W. Rehman, M. Waseem, A. Khan, H. Shaheen, Materials Research Express, 8(7), 075009, (2021); https://doi.org/10.1088/2053-1591/ac1187

[48] S. Asaithambi, P. Sakthivel, M. Karuppaiah, K. Balamurugan, R. Yuvakkumar, M. Thambidurai, G. Ravi, Journal of Alloys and Compounds, 853, 157060, (2021); https://doi.org/10.1016/j.jallcom.2020.157060

[49] X. Zhao, X. Ma, Q. Lu, Q. Li, C. Han, Z. Xing, X. Yang, Electrochimica Acta, 249, 72, (2017); https://doi.org/10.1016/j.electacta.2017.08.004

[50] Q. Lu, Z. Wei, J. Liang, C. Li, L. Li, J. Ma, ChemistrySelect, 7(6), e202102794, (2022).

[51] X. Leng, Y. Wang, F. Wang, Journal of Physics: Conference Series, 1407(1), 012070, (2019); https://doi.org/10.1088/1742-6596/1407/1/012070

[52] H. Peng, J. Lu, C. Wu, Z. Yang, H. Chen, W. Song, P. Li, H. Yin, Applied Surface Science 353, 1003, (2015); https://doi.org/10.1016/j.apsusc.2015.06.178

[53] P. Falcaro, F. Normandin, M. Takahashi, P. Scopece, H. Amenitsch, S. Costacurta, C. M. Doherty, J. S. Laird, M. D. H. Lay, F. Lisi, A. J. Hill, D. Buso, Advanced Materials, 23(34), 3901, (2011); https://doi.org/10.1002/adma.201101233

[54] W. Zhao, Z. Ghorannevis, L. Chu, M. Toh, C. Kloc, P. Tan, G. Eda, ACS nano, 7(1), 791, (2013); https://doi.org/10.1021/nn305275h

[55] L. Muscuso, S. Cravanzola, F. Cesano, D. Scarano, A. Zecchina, The Journal of Physical Chemistry C, 119(7), 3791, (2015); https://doi.org/10.1021/jp511973k

[56] Y. Kim, D. Lee, S. Y. Kim, E. Kang, C. K. Kim, Nanomaterials, 9(7), 927, (2019); https://doi.org/10.3390/nano9070927

[57] T. Cassagneau, J. H. Fendler, T. E. Mallouk, Langmuir, 16(1), 241, (2000); https://doi.org/10.1021/la990776h

[58] B. D. Viezbicke, S. Patel, B. E. Davis, D. P. Birnie, physica status solidi, 252(8), 1700, (2015); https://doi.org/10.1002/pssb.201552007

[59] Y. J. Yuan, H. W. Lu, Z. T. Yu, Z. G. Zou, ChemSusChem, 8(25), 4113, (2015); https://doi.org/10.1002/cssc.201501203

[60] A. Ramasubramaniam, Physical Review B, 87(19), 195201, (2013); https://doi.org/10.1103/PhysRevB.87.195201

[61] I. Khan, K. Saeed, I. Zekker, B. Zhang, A. H. Hendi, A. Ahmad, S. Ahmad, N. Zada, H. Ahmad, L. A. Shah, T. Shah, I. Khan, Water, 14(2), 242, (2022); https://doi.org/10.3390/w14020242

[62] K. Ravichandran, R. Uma, S. Sriram, D. Balamurgan, Ceramics International, 43(13), 10041, (2017); https://doi.org/10.1016/j.ceramint.2017.05.020

[63] F. Ye, H. Li, H. Yu, S. Chen, X. Quan, Applied Surface Science, 426, 177, (2017); https://doi.org/10.1016/j.apsusc.2017.07.087

[64] J. Lv, R. Miao, M. Zhang, G. He, M. Zhao, B. Yu, W. Wang, B. Li, Z. Sun, Journal of Materials Science: Materials in Electronics, 29, 16282, (2018); https://doi.org/10.1007/s10854-018-9717-5

[65] K. C. Lalithambika, K. Shanmugapriya, S. Sriram, Applied Physics A, 125, 1, (2019); https://doi.org/10.1007/s00339-019-3120-9